

Revealing the complex sulfur reduction mechanism using cyclic voltammetry simulation

Patrick Schön^a, Ulrike Krewer^{b,*}

^a Technische Universität Braunschweig, Institute of Energy and Process Systems Engineering, Franz-Liszt-Straße 35, Braunschweig 38106, Germany

^b Karlsruhe Institute of Technology, Institute for Applied Materials – Electrochemical Technologies, Adenauerring 20b, Karlsruhe 76131, Germany

ARTICLE INFO

Keywords:

Chemical disproportionation
Transport and kinetic parameters
CV Modeling

ABSTRACT

Understanding the complex reaction mechanism and kinetics of sulfur reduction is prerequisite to design well performing lithium-sulfur batteries. Decoupling of individual polysulfide species is problematic when only using experimental methods. Model supported electrochemical analysis together with HPLC-MS analysis of the reacting species is used to compensate for this missing insight, as it enables to analyze the underlying species, transport, kinetic and thermodynamic processes. Concentration measurements confirm a strong prevalence of chemical equilibrium reactions that cause many species to be present over a wide range of SoC. An EEC-mechanism represents the top-down view and yields the simplest generic mechanism, that is able to reproduce the electrochemical behavior. Reduction of sulfur is performed by two consecutive electron transfer reactions while a chemical reaction accounts for the decreasing cathodic-to-anodic peak ratio with decreasing scan rate. A physically motivated E3C4-mechanism is shown to yield convincing results besides transport and kinetic parameters. Circular routes and chemical equilibrium are included to reproduce all characteristics of the experimental cyclic voltammogram. Influence of kinetic and transport parameters are elucidated with a global sensitivity analysis. Peak currents are almost exclusively influenced by electrochemical kinetics, while diffusion limited currents largely depend on transport parameters. In addition, the E3C4-mechanism reveals the prominent role of chemical equilibrium between polysulfides in the range of transport limitation. The revealed mechanistic complexity leads to complex, non-intuitive behavior of sulfur electrodes and Li-S batteries. Thus it is highly recommended to use the presented E3C4 kinetics and model for a more reliable interpretation of experimental behavior, including the dynamic relaxation behavior, and for improved electrode and cell design that takes chemical disproportionation into account.

1. Introduction

Lithium-sulfur batteries (LSBs) practically obtain gravimetric energy densities of $\sim 600 \text{ Whkg}^{-1}$ on cell level [1]. They have the potential to outperform current lithium-ion batteries in terms of gravimetric energy density [2,3] and are advantageous due to low cost of raw active material, its high abundance and low toxicity. It has a milder environmental impact and can be handled more safely [4].

However, significant technical challenges persist. Among these are the high solubility of polysulfide intermediates into the electrolyte that causes the polysulfide shuttle phenomenon [5,6] resulting in serious degradation on the electrodes, reduction of coulombic efficiency and loss of active material. Cycle life is further

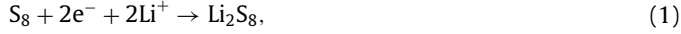
limited by surface passivation due to deposition of poorly soluble products (e.g. Li_2S_2 , Li_2S) at the cathode and polysulfide reaction with the electrolyte [7]. It is clear that the complex reaction mechanism involving electrochemical and chemical reactions, precipitation and dissolution of solid species is central to all these problems and thus limits the power capability of present LSBs. It is experimentally extremely difficult to decouple individual polysulfide species, so the elucidation of mechanistic steps is problematic [8]. In addition, the solubility and reaction mechanism of intermediate sulfide ions depends on the solvent used in the electrolyte, and so does the electrochemical behavior of the cell [9,10]. The reaction pathways also change as a function of state of charge (SoC) [11].

Wild et al. [12] summarized several experimental and simulation studies, deriving a representative reaction mechanism for the discharge of a LSB. The experimentally observable high plateau at $>2.3\text{V}$ is characterized by a two step reduction:

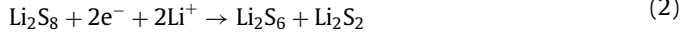
* Corresponding author.

E-mail address: ulrike.krewer@kit.edu (U. Krewer).

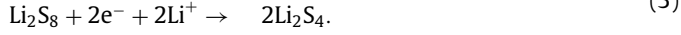
The reduction of sulfur,



and the subsequent reductive dissociation,



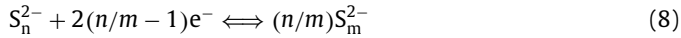
or



The low plateau at ca. 2.1V is suggested to be dominated by chemical equilibrium of the LiS_3 radical (Eq. 4) as well as its reduction (Eq. 5).



Wild et al. [12] mentions diverse possible association and precipitation reactions as in Eq. 6, which are not covered in this equation set. This represents the common reaction pathway of the investigated studies. Still the exact pathway has not been proposed by any of the examined studies. Therefore, all possible reactions should be taken into account when investigating the reaction mechanism, which can be summarized as discussed in our previous study [11].

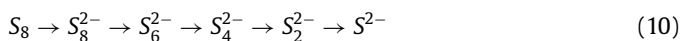


where $\{n|n \in \mathbb{N}, 2 \geq n \leq 8\}$ and $\{m|m \in \mathbb{N}, 1 \geq m \leq 7, m < n, m \geq 1\}$. The chemical disproportionation reactions are suggested to follow the general reaction scheme:



where $\{n|n \in \mathbb{N}, 2 \geq n \leq 7\}$, $\{m|m \in \mathbb{N}, 2 \geq m \leq 7, m \leq n\}$ and $\{x|x \in \mathbb{N}, 1 \geq x \leq 3, x \leq n - 8, x \leq 1 - m\}$.

Modeling of LSBs is a fundamental demand within development and is vital for applications [12,13]. For example, capacity determination under current load is only possible through the application of advanced battery modeling and estimation techniques to determine current state and predict remaining useful life. In addition, battery modeling enables to ensure safe charging and discharging, optimal utilization of batteries, fast charging and other applications. Several modeling approaches have been made to enlighten different aspects of the LSB reaction mechanism, kinetics and transport properties. For example temperature dependency of state of charge [14], transport limitations [15], shuttle mechanism [16] and precipitation/dissolution [17] have been investigated. An important aspect that is mostly unattended so far is the reaction mechanism. In general, a consecutive reduction of sulfur to increasingly short polysulfides has been assumed in modeling [5,18–20].



Discrimination using steady-state curves is almost impossible due to too many parameters with insufficient data. This can be done by dynamic experiments. These allow to distinguish between slow and fast processes. They also have not been used for sulfur reduction kinetic identification so far. However, dynamic methods with comparison of experimental and modeling results have shown

great potential in identifying characteristics of reaction mechanisms and kinetics in other context. For methanol oxidation using electrochemical impedance spectroscopy [21], for oxygen reduction using nonlinear frequency responses [22], or even microbial glucose and acetate oxidation [23]. The latter study also presented a parameter sensitivity analysis and parameter identifiability study to identify parameter dependencies and reliability of the model and model parameters. A similar approach should be followed in this work to identify a credible mechanism and kinetics. This will allow for better understanding of LSBs and interpretation of experiments, e.g. relaxation phenomena. It allows to develop solutions to tackle the challenges to LSBs mentioned in the intro of this paper. Therefore, a model supported analysis of the reaction mechanism using cyclic voltammetry (CV) in combination with sensitivity analysis is used to give significant additional insights into the electron transfer and chemical reaction routes besides a robust kinetic model.

We base our approach on our dynamic CV experiments that revealed significant changes in the CV with SoC and scan rate [11]. A 1-d physicochemical model is used to show the interaction of reaction and transport processes causing the experimentally observed CV and species concentrations [11], and to identify a feasible mechanism and kinetics of the Li/S electrode. The implemented mechanism contains the results of latest published scientific knowledge. We reveal reaction currents, concentrations and reaction rates and their evolution over time and distance to the electrode surface. In addition, a global sensitivity analysis is performed to reveal the impact of transport and kinetic parameters on the current, i.e. electrode performance [24–26].

We analyze two different scenarios, (i) an EEC_{irr}-mechanism as simple generic mechanism to evaluate its applicability to give insights to the LSB mechanism and (ii) a physically motivated, E3C4-mechanism to elucidate different aspects of the reaction mechanism regarding reaction routes, transferred electrons and importance of transport in detail.

2. Model

The modeled system consists of a static graphite working electrode immersed in a stagnant solution containing the electrochemically active cyclic octasulfur (S_8) as well as an excess of supporting electrolyte. The electron transfer reactions of S_8 and polysulfides take place at the surface of the working electrode. Chemical reactions take place in the electrolyte. Finally, the counter electrode completes an electrical circuit with the working electrode.

A chemical gradient will exist as a consequence of the different concentrations of the electrochemically active species depending on the distance to the electrode surface. The system will respond in order to balance the concentration gradient with the corresponding flux of material by diffusion. For typical electrochemical experiments, where a very large number of molecules are involved, the diffusion process can be described by the statistical Ficks laws [27] which accounts for the changes in concentration with time and location. Compared to the thickness of the diffusion layer $\delta \sim \sqrt{Dt}$ where D is the largest diffusion coefficient and t is the maximum simulated time, the area of the electrode is large, therefore a one dimensional approach is applicable.

The problem is thus reduced to one spatial dimension, x , which is the distance normal to the flat surface of the electrode. Also, transport by ion migration in the electric field is eliminated by assuming an excess of electrolyte. In addition, the electrolyte is non-reactive, the environment is isotherm and substrates have a homogeneous concentration at the beginning of the simulation. Fig. 1 illustrates the electrode with the underlying processes.

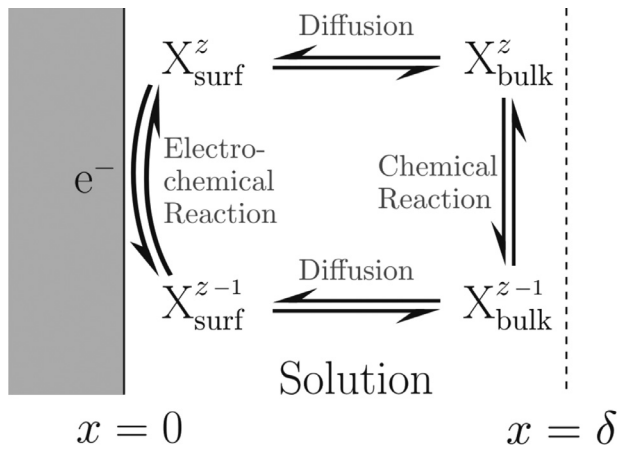


Fig. 1. Illustration of modeled transport and kinetic processes implemented in the 1d-physicochemical model.

Modeling of electrode kinetics for CV simulation

An appropriate model for CV is required to obtain information about more complex reaction kinetics where no analytical solution is available. Current CV simulation programs, either commercial [28–30] or open source [31–33], lack in functionality and flexibility for the desired investigations. Therefore, a new implementation is realized.

Cyclic voltammetry

At any time t on the forward sweep, the potential, E , is given by

$$E = E_{\text{init}} - \nu t \quad (11)$$

with E_{init} the initial potential and ν the scan rate. At any time $t = t_{\text{switch}}$, the potential reaches the vertex potential E_{ν} where the sweep direction reverses. For $2t_{\text{switch}} > t > t_{\text{switch}}$,

$$E = E_{\nu} + \nu(t - t_{\text{switch}}). \quad (12)$$

Kinetic and transport equations

In general, the conservation of mass equation to describe the motion of charged chemical species in a fluid medium is described by the Nernst-Planck equation. In this particular case, migration due to electrostatic forces is neglected, and convection can also be neglected because the fluid has no velocity. Therefore, transport is described by diffusion. In addition to transport, a source term, S , is added to account for chemical reactions in the electrolyte. This yields the following mass balance for charged and neutral species:

$$\frac{\partial c_i}{\partial t} = D_i \frac{\partial^2 c_i}{\partial x^2} + S_i \quad (13)$$

with c_i the concentration of species i , t the time, D_i the diffusion coefficient of species i . The time dependency of the source term is only due to local chemical reactions. Volume specific chemical reaction rates, r_j , follow mass action law:

$$r_j = k_{j,f} \prod_{i_{\text{ed}}} c_i^{v_{i,j}} - k_{j,b} \prod_{i_{\text{prod}}} c_i^{v_{i,j}} \quad (14)$$

with k_j the reaction rate constant of the forward (f) and backward (b) portion of reaction j , $v_{i,j}$ the stoichiometric coefficient of species i in the reaction j participating as an educt of a reaction (ed) or a product of a reaction (prod). The source term S_i of each species i will consequently be the sum of all reaction rates of reactions where the species is participating:

$$S_i = \sum_{j=1}^R \frac{v_{i,j} r_j}{\Delta x}. \quad (15)$$

with Δx the size of the first element normal to the electrode surface. The boundary condition contains the electron transfer reactions at the electrode/electrolyte interface:

$$\left(-D_i \frac{\partial c_i}{\partial x} \right)_{x=0} = \sum_i v_{i,j} \frac{i_j}{n_j F} \quad (16)$$

with i_j the partial current density for electron transfer reaction j , n the number of transferred electrons and F the Faraday constant. The condition at the bulk boundary is:

$$\left(-D_i \frac{\partial c_i}{\partial x} \right)_{x=\delta} = 0. \quad (17)$$

Applying Faraday's law, the partial current density i_j of multiple electron transfer reactions is calculated by:

$$i_j = -n_j F r_{j,\text{el}} \quad (18)$$

with n_j the number of electrons transferred and $r_{j,\text{el}}$ the electrochemical reaction rate.

The electrochemical reaction rate constants show an exponential dependence with the applied potential, according to the Butler-Volmer model. Only one electron can be transferred at a time to calculate the current density i [34]. Hence, for a given reaction, $n = 1$ is assumed in the exponent. Therefore, in case of electron transfer reactions the reaction rate constant of the forward reaction $k_{j,\text{f,el}}$ and the backward reaction $k_{j,\text{b,el}}$ are defined as:

$$k_{j,\text{f,el}} = k_{j,\text{f,el}}^* \exp\left(\frac{a_j F}{RT} (E - E_{f,0j})\right) \quad (19)$$

$$k_{j,\text{b,el}} = k_{j,\text{b,el}}^* \exp\left(-\frac{(1 - \alpha_j) F}{RT} (E - E_{f,0j})\right)$$

with α_j the charge transfer coefficient, R the molar gas constant, T the temperature, E the potential and $E_{f,0j}$ the formal potential. As a result, the reaction current i_j can be determined by:

$$i_j = -n_j F \left(k_{j,\text{f,el}}^* \exp\left(\frac{\alpha_j F}{RT} (E - E_{f,0j})\right) \prod_{i_{\text{ed}}} c_i^{v_{i,j}} - k_{j,\text{b,el}}^* \exp\left(-\frac{(1 - \alpha_j) F}{RT} (E - E_{f,0j})\right) \prod_{i_{\text{prod}}} c_i^{v_{i,j}} \right). \quad (20)$$

The sum of partial current densities yields the total current density i :

$$i = \sum_{j=1}^R i_j \quad (21)$$

Initial concentrations

At the initial state, all involved species are in equilibrium. The concentrations can be obtained by solving an equation system of Nernst equations for each electron transfer reaction for the initial potential:

$$E_j = E_{f,0j} + \frac{RT}{F} \ln \prod_i c_i^{v_{i,j}}. \quad (22)$$

Unequally spaced grid

An exponentially expanding grid with smaller grid size close to the electrode was used to account for larger gradients close to the electrode/electrolyte interface [35]. Expansion is defined according to:

$$\Delta x_{fq} = \Delta x_{f0} W^q \quad (23)$$

with Δx_f the size of modeled volume element, w the growth factor and q the volume element ($q = 1$ at the interface). w is restricted by the distance between electrolyte and bulk, L :

$$L = \sum_{q=1}^Q \Delta x_{fq} \quad (24)$$

with Q the total number of volume elements.

Solving the partial differential equation system

In order to solve the ordinary differential equation system, the CVode solver, which was first introduced by Cohen et al. [36] and implemented by Hindmarsh et al. [37] in the Suite of Nonlinear and Differential/Algebraic Equation Solvers, is applied. The most suitable numerical integration method for this set of equations are the Backward Differentiation Formulas [38]. The generalized minimal residual method [39] is used as linear solver type. Absolute tolerances are 1×10^{-16} while relative tolerances are 1×10^{-6} . Convergence of the solution, especially regarding grid parameters was confirmed as refining the parameters lead to no visual changes of the CVs. The programming interface for Python of this solver is provided by the Assimulo package [40].

Sensitivity analysis

To evaluate sensitivities of the CVs to parameters, a variance-based global sensitivity analysis was applied [24,25]. Through this global sensitivity analysis, the variance of the output of the system is decomposed into fractions, which can be attributed to model parameters or sets of model parameters. These fractions, so called Sobol indices, are directly interpreted as values of sensitivity that are measured across the whole input space [26]. This method also allows to reveal correlations between parameters. The first-order sensitivity index, Φ_i , measures the direct variance-based sensitivity. This is the contribution to the output variance of the main effect of an examined parameter, therefore it measures the effect of varying this parameter alone, but averaged over variations in other input parameters. It is normalized by the total variance to provide a fractional contribution. The sum of first- and higher-order interaction indices $\Phi_{i,j}$, $\Phi_{i,j,k}$, ... implicates that,

$$\sum_{i=1}^d \Phi_i + \sum_{i<j}^d \Phi_{i,j} + \dots + \Phi_{1,2,\dots,d} = 1. \quad (25)$$

In order to calculate the variance, the number of samples is calculated by $N(2D + 2)$, with D the number of model inputs, where in this study the argument N is set to be 1000 [24–26]. The Python implementation of the sensitivity analysis is realized in the SALib package [41].

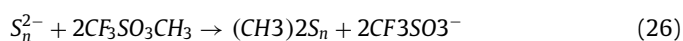
3. Experiment

Here we complement the experimental CVs [11] with measurements of chemical composition of the solution in the same setup to motivate the chosen mechanism and species. With high performance liquid chromatography (HPLC) polysulfides are separated depending on their chain lengths and each dimethyl polysulfide can be identified based on the monotonous relationship between retention time and chain length [42–47]. Except for sulfide (S^{2-}), all polysulfide ions and elemental sulfur can be separated and identified by HPLC-mass spectrometry (MS) after derivatization [43,48].

Experimental set-up

A lithium sulfur cell was established using the experimental setup by Schön et al. [11]. A glassy carbon electrode with

a flat round tip with an area of 0.196cm^2 (Pine Research Instrumentation, Durham, NC) was used as working electrode. The counter electrode was prepared using lithium (Li) foil (99.9%, Merck KGaA). The electrodes were immersed in 15mL liquid electrolyte consisting of lithium bis(trifluoromethanesulfonyl)imide (LiTFSI) (SigmaAldrich) 1mol in a 1:1 mixture of 1,3-Dioxolan (DOL) (SigmaAldrich)/1,2-dimethoxyethan (DME) (SigmaAldrich). Cyclic octasulfur (99.9%, Merck KGaA) was added as active material with a concentration of 4mmol. Galvanostatic discharge is used to investigate the discharge at a constant current density of 3.57Am^{-2} , until a potential of 0.6V is reached to ensure deep discharge. A Gamry Reference 3000 is used as galvanostat. After reaching this limit the discharge was terminated. $200\mu\text{L}$ of electrolyte is taken out of the cell at different SoC, at 100%, 87.1%, 40.3% and 0% SoC. The second sample is taken at the higher potential discharge plateau and the third at the lower potential discharge plateau (see Fig. A.12). Immediate derivatization using the established method of Kamysny et al. [49] is performed by adding $350\mu\text{L}$ methanol and $50\mu\text{L}$ methyl trifluoromethansulfonate (MeOTf) (99.9%, Sigma Aldrich). The occurring reaction follows Eq. (26):



Experimental results

The chromatogram at 100% SoC (Fig. 2a) shows two peaks. The first peak with a retention time of 21.2min is identified as DOL and the second peak with a retention time of 35min is identified as S_8 . The absence of other peaks assures that no polysulfides are present at the beginning of galvanostatic discharge. Analyzing the chromatogram at 87.1% SoC, seven additional peak are observed and generation of polysulfides can therefore be confirmed. Except for the fourth and the last peak, all peaks are present until the end of discharge, as seen in Fig. 2c and d. In addition, an increase in these peaks area can be observed throughout galvanostatic discharge. At the same time the S_8 peak decreases in peak area (Fig. A.12).

The identification of polysulfides is done by the combined results of three different techniques: (i) comparison of the retention times of standards, (ii) confirmation that polysulfides are present via MS, (iii) correlation of retention times with polysulfide chain lengths [42–47].

The S_8 peak area decreases from 100% to 33.2%, while the relative area of different polysulfides increases during the galvanostatic discharge. CV validates, that the electron transfer reaction of S_8 to octasulfide (S_8^{2-}) and further to tetrasulfide (S_4^{2-}) have a high formal potential. This results in a fast consumption of S_8 at the higher potential discharge plateau, which can also be confirmed by measuring the concentrations. Finally, S_8 concentration is still decreasing, when the electron transfer reactions yield a much lower mixed potential. This proves the presence of chemical reactions that consume S_8 at the lower potential discharge plateau.

Concentrations of polysulfides cannot be quantified because standards are unavailable. Multiple short chain polysulfide ions are produced during electrochemical reduction of S_8 , of which trisulfide (S_3^{2-}) and S_4^{2-} are the main products. Fig. A.13 shows that the decrease of S_8 and increase of polysulfides is highest at the beginning and is slowing down during the experiment. This supports the assumption of the important role of disproportionation reactions. The polysulfide increase is higher at the higher potential discharge plateau compared to the lower potential discharge plateau, indicating that S^{2-} was produced at the end of the higher potential discharge plateau, which is not analyzed by HPLC-MS. Overall, the results of the chemical analysis confirms the assumptions of the reaction mechanism from Schön et al. [11].

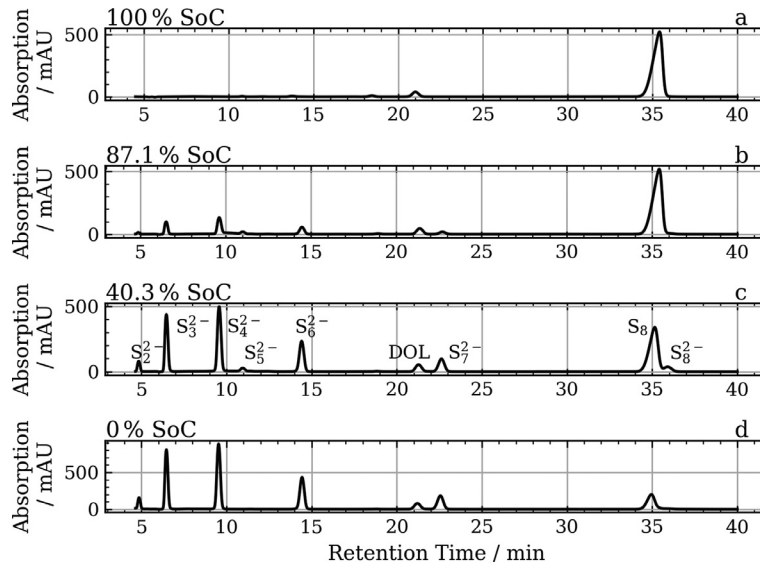


Fig. 2. Chromatograms of separated polysulfides at different states of charge.

4. Reaction mechanisms and governing equations

Two reaction mechanisms are evaluated in the following towards their applicability to reproduce the experimental electrochemical behavior. The first mechanism represents the simplest generic option to reproduce the main characteristic features of the CV from a top-down view, with only the electrochemical result as foundation, and is an EEC_{irr} -mechanism. The second is named E3C4-mechanism containing three electron transfer and four chemical reactions, which allows to analyze all characteristics of the CV, but at the expense of higher complexity. The chemical and electron transfer reactions implemented in the E3C4-mechanism were chosen bottom-up with the foundation of physical plausibility.

EEC-mechanism

In the first scenario, the experimental CV data is analyzed by a mechanism containing two reversible electron transfer steps followed by an irreversible chemical reaction, which is known as EEC_{irr} -mechanism. This mechanism is derived from the experimental results, where two phenomena are obvious: (i) Two cathodic peaks that originate from at least two electron transfer steps, and (ii) a decreasing anodic to cathodic peak current ratio with decreasing scan rate. The two cathodic peaks lead to the assumption of two electron transfer reactions with different formal potentials. For the total electron transfer in the potential window of 3.8V to 1V, Lu et al. [10] propose a transfer of $5.4 e^- \text{ mol}_{S_8}^{-1}$. This is applied to the first electron transfer reaction Ia. The second electron transfer reaction IIa causes the second reduction peak, where two electrons are assumed to be transferred, giving the correct current response for the second peak. The decreasing peak ratio is assumed to be caused by a chemical reaction that consumes reactants that otherwise oxidize by the anodic electron transfer reaction. The irreversible step can indicate precipitation reaction of S^{2-} . As the reactions are empirically derived, X and Y are used instead of S_8 and polysulfide species. As a result the reaction mechanism is defined as:



Reduction of X results in the product $X^{5.4-}$ by consecutively transferring $5.4e^-$ from the electrode to the species. The amount of $5.4e^-$ is the accumulated sum of electrons that are transferred per mole of X. Here, underlying consecutive elementary reaction steps with single electron transfer are assumed with the last step being rate limiting. The same assumption holds for the reduction of $X^{5.4-}$ to $X^{7.4-}$, where only the slower of the two one-electron transfer reactions defines the reaction rate. Reversing the scan direction, does not change the hypothesis since these electron transfer steps are assumed to be reversible. This leads to the mass balances and kinetic equations system in Tab. 1 according to the described physicochemical model.

E3C4-Mechanism

A majority of literature publications propose electron transfer reactions, where four electrons are transferred during two consecutive electron transfer steps, reducing S_8 (reaction Ib) and S_8^{2-} (reaction IIb) [10,43–45,50]. This finding is confirmed by the conducted CV studies [11] and the HPLC studies described in the previous section. In this context it seems quite unrealistic, that $5.4e^-/\text{mol}_{S_8}$ transfer always jointly as assumed in the EEC_{irr} -mechanism. And as the mechanism cannot cover the variety of identified species, the more physically motivated E3C4-mechanism is investigated. Compared to the EEC_{irr} -mechanism, less electrons are transferred during the first two reduction steps. The missing electrons per mole S_8 , that would therefore deliver a lower current, are supposed to be compensated by circular routes due to chemical reactions forming new S_8 (reaction Vb) [51]. The relaxation behavior of the investigated cell during open circuit potential (OCP) measurement [11], as well as the decreasing S_8 consumption at lower SoC during discharge, which is measured by HPLC (Fig. A.13), confirms the presence of such reaction. Chemical reactions of short chain polysulfides that mainly involve S_4^{2-} to disulfide (S_2^{2-}) in reaction VIb and VIIb are also included taking into account the main products of HPLC analysis. The broad CV peaks at lower SoC [11] result because S_4^{2-} which is responsible for the reduction at the lower potential discharge plateau (IIb), is strongly involved in these chemical reactions (IVb, Vb, VIb), that

Table 1
Mass balances and kinetic equation system of the EEC_{irr}-mechanism.

Mass balances in the electrolyte:	Boundary conditions:
$\frac{\partial c_X}{\partial t} = D_X \frac{\partial^2 c_X}{\partial x^2}$ (27)	$\left(-D_X \frac{\partial c_X}{\partial x}\right)_{x=0} = \frac{i_{ib}}{z_{ib}F}$ (31)
$\frac{\partial c_{X^{5.4}}}{\partial t} = D_{X^{5.4}} \frac{\partial^2 c_{X^{5.4}}}{\partial x^2}$ (28)	$\left(-D_{X^{5.4}} \frac{\partial c_{X^{5.4}}}{\partial x}\right)_{x=0} = -\frac{i_{ib}}{z_{ib}F} + \frac{i_{IIa}}{z_{IIa}F}$ (32)
$\frac{\partial c_{X^{7.4}}}{\partial t} = D_{X^{7.4}} \frac{\partial^2 c_{X^{7.4}}}{\partial x^2} - k_{f,IIIa} c_{X^{7.4}}$ (29)	$\left(-D_{X^{7.4}} \frac{\partial c_{X^{7.4}}}{\partial x}\right)_{x=0} = -\frac{i_{ib}}{z_{ib}F}$ (33)
$\frac{\partial c_Y}{\partial t} = D_Y \frac{\partial^2 c_Y}{\partial x^2} + k_{f,IIIa} c_{X^{7.4}}$ (30)	The remaining flux terms at the boundaries $x = 0$ and $x = \delta$ are zero.
Partial currents of electron transfer reactions Ia and IIa	
$i_{Ia} = z_{Ia} F k_{Ia} \left(\exp\left(\frac{\alpha_{Ia} F}{RT} (E - E_{f,Ia}^0)\right) c_{X^{5.4}} - \exp\left(-\frac{(1-\alpha_{Ia}) F}{RT} (E - E_{f,Ia}^0)\right) c_X \right)$ (34)	
$i_{IIa} = z_{IIa} F k_{IIa} \left(\exp\left(\frac{\alpha_{IIa} F}{RT} (E - E_{f,IIa}^0)\right) c_{X^{7.4}} - \exp\left(-\frac{(1-\alpha_{IIa}) F}{RT} (E - E_{f,IIa}^0)\right) c_{X^{5.4}} \right)$ (35)	
Total reaction current:	
$i = i_{Ia} + i_{IIa}$ (36)	

Table 2
Mass balances and kinetic equation system of the E3C4-mechanism.

Mass balances in the electrolyte:	Reaction rates:
$\frac{\partial c_{S_8}}{\partial t} = D_{S_8} \frac{\partial^2 c_{S_8}}{\partial x^2} + r_{Vb}$ (37)	$r_{IVb} = k_{f,IVb} c_{S_8^4} - k_{b,IVb} c_{S_2^2}^2$ (44)
$\frac{\partial c_{S_8^2}}{\partial t} = D_{S_8^2} \frac{\partial^2 c_{S_8^2}}{\partial x^2}$ (38)	$r_{Vb} = k_{f,Vb} c_{S_4^2}^3 - k_{b,Vb} c_{S_8} c_{S_2^2}^2$ (45)
$\frac{\partial c_{S_4^4}}{\partial t} = D_{S_4^4} \frac{\partial^2 c_{S_4^4}}{\partial x^2} - r_{IVb}$ (39)	$r_{VIIb} = k_{f,VIIb} c_{S_2^2}^2 - k_{b,VIIb} c_{S_2^2} c_{S_2^2}$ (46)
$\frac{\partial c_{S_4^2}}{\partial t} = D_{S_4^2} \frac{\partial^2 c_{S_4^2}}{\partial x^2} + 2r_{IVb} - 3r_{Vb} + r_{VIIb}$ (40)	$r_{VIIIb} = k_{f,VIIIb} c_{S_2^2}^2 - k_{b,VIIIb} c_{S_2^2} c_{S_2^2}$ (47)
Boundary conditions:	
$\frac{\partial c_{S_2^2}}{\partial t} = D_{S_2^2} \frac{\partial^2 c_{S_2^2}}{\partial x^2} - 2r_{Vb} + r_{VIIb}$ (41)	$\left(-D_{S_8} \frac{\partial c_{S_8}}{\partial x}\right)_{x=0} = \frac{i_{Ib}}{z_{Ib}F}$ (48)
$\frac{\partial c_{S_2^4}}{\partial t} = D_{S_2^4} \frac{\partial^2 c_{S_2^4}}{\partial x^2} + r_{Vb} + r_{VIIb} - 2r_{VIIIb}$ (42)	$\left(-D_{S_8^2} \frac{\partial c_{S_8^2}}{\partial x}\right)_{x=0} = -\frac{i_{Ib}}{z_{Ib}F} + \frac{i_{IIb}}{z_{IIb}F}$ (49)
$\frac{\partial c_{S_2^2}}{\partial t} = D_{S_2^2} \frac{\partial^2 c_{S_2^2}}{\partial x^2} + 2r_{Vb} + r_{VIIIb}$ (43)	$\left(-D_{S_4^4} \frac{\partial c_{S_4^4}}{\partial x}\right)_{x=0} = -\frac{i_{Ib}}{z_{Ib}F}$ (50)
	$\left(-D_{S_4^2} \frac{\partial c_{S_4^2}}{\partial x}\right)_{x=0} = \frac{i_{IIb}}{z_{IIb}F}$ (51)
	$\left(-D_{S_2^2} \frac{\partial c_{S_2^2}}{\partial x}\right)_{x=0} = -2 \frac{i_{IIIb}}{z_{IIIb}F}$ (52)
	The remaining flux terms at the boundaries $x = 0$ and $x = \delta$ are zero.
Partial currents of electron transfer reactions Ib, IIb and IIIb:	
$i_{Ib} = z_{Ib} F \Delta x_1 k_{Ib} \left(\exp\left(\frac{\alpha_{Ib} F}{RT} (E - E_{f,Ib}^0)\right) c_{S_8^2} - \exp\left(-\frac{(1-\alpha_{Ib}) F}{RT} (E - E_{f,Ib}^0)\right) c_{S_8} \right)$ (53)	
$i_{IIb} = z_{IIb} F \Delta x_1 k_{IIb} \left(\exp\left(\frac{\alpha_{IIb} F}{RT} (E - E_{f,IIb}^0)\right) c_{S_4^2} - \exp\left(-\frac{(1-\alpha_{IIb}) F}{RT} (E - E_{f,IIb}^0)\right) c_{S_8^2} \right)$ (54)	
$i_{IIIb} = z_{IIIb} F \Delta x_1 \left(k_{IIIb,f,el} \exp\left(\frac{\alpha_{IIIb} F}{RT} (E - E_{f,IIIb}^0)\right) c_{S_2^2}^2 - k_{IIIb,b,el} \exp\left(-\frac{(1-\alpha_{IIIb}) F}{RT} (E - E_{f,IIIb}^0)\right) c_{S_2^2}^2 \right)$ (55)	
Total reaction current:	
$i = i_{Ib} + i_{IIb} + i_{IIIb}$	

have been previously proposed [43,44]. The proposed mechanism is as follows:



This reaction mechanism leads to the mass balances and kinetic equation system in Tab. 2.

5. Parameterization

EEC-mechanism

Following the experimental conditions, the starting concentration of reactant X is 4mmol, and initial concentrations of $X^{5.4-}$, $X^{7.4-}$ and Y are zero. The temperature is set to 293.15K. The diffusion parameters are taken from Lu et al. [10] where rotating ring-disk electrode measurements revealed a value of $2.6 \times 10^{-10} \text{ m}^2 \text{ s}^{-1}$ for sulfur in 1:1 DOL:DME with 1M LiTFSI. Charge transfer coefficients for each of the electron transfer reactions are chosen to be 0.5. Following the experimental procedure, CV is simulated for two cycles in a range between 3.8V to 1.0V whereas the evaluated part of the CV is the second cycle. At potentials lower than 1.8V the experimental results show undesired side reactions of the electrolyte, that are not included in the model. Diffusion coefficients $D_{X^{5.4-}}$, $D_{X^{7.4-}}$, D_Y , as well as reaction constants k_{Ia} and k_{IIa} , formal potentials $E_{f,Ia}^0$ and $E_{f,IIa}^0$ of the electron transfer reactions and the reaction constants of the chemical reaction $k_{f,IIIa}$ and $k_{b,IIIa}$ are identified using a least square approach on the experimental CV at 100mVs⁻¹. They are given in Tab. 3.

Table 3
Identified parameters for the EEC_{irr}-mechanism.

D_X	$D_{X^{5.4}}$	$D_{X^{7.4}}$	D_Y
m^2s^{-1}	m^2s^{-1}	m^2s^{-1}	m^2s^{-1}
$2.60e-10$	$7.6e-10$	$1.25e-9$	$3.64e-10$
$E_{f,IIa}$	$E_{f,IIIa}$	k_{Ia}	k_{IIa}
V	V	ms^{-1}	ms^{-1}
2.44	2.20	5.73×10^{-10}	1.64×10^{-10}
$k_{f,IIIa}$	$k_{b,IIIa}$		
s^{-1}	s^{-1}		
1.13×10^{-10}	0		

Table 4
Identified parameters for the E3C4-mechanism.

D_{S_8}	$D_{S_8^2}$	$D_{S_8^4}$	$D_{S_4^2}$
m^2s^{-1}	m^2s^{-1}	m^2s^{-1}	m^2s^{-1}
2.6×10^{-10}	2.6×10^{-10}	2.6×10^{-10}	7.6×10^{-10}
$D_{S_8^2}$	$D_{S_8^2}$	$D_{S_8^2}$	$E_{f,IIb,IIIb}$
m^2s^{-1}	m^2s^{-1}	m^2s^{-1}	V
9×10^{-10}	1.25×10^{-10}	1×10^{-11}	2.44
$E_{f,IIIb}$	$k_{f,IIb}$	$k_{f,IIIb}$	$k_{b,IIIb}$
V	ms^{-1}	ms^{-1}	$(m^3mol^{-1})ms^{-1}$
2.3	2×10^{-6}	7×10^{-8}	7×10^{-8}
$k_{f,IVb}$	$k_{b,IVb}$	$k_{f,Vb}$	$k_{b,Vb}$
s^{-1}	$m^3mol^{-1}s^{-1}$	$(m^3mol^{-1})^2ms^{-1}$	$(m^3mol^{-1})^2ms^{-1}$
3.75	15	1	4
$k_{f,VIIb}$	$k_{b,VIIb}$	$k_{f,VIIIb}$	$k_{b,VIIIb}$
$(m^3mol^{-1})ms^{-1}$	$(m^3mol^{-1})ms^{-1}$	$(m^3mol^{-1})ms^{-1}$	$(m^3mol^{-1})ms^{-1}$
0.5	0.5	1	1

E3C4-mechanism

The starting concentration of S_8 is set to 4mmol, and initial concentrations of the remaining species are set to zero. The temperature is set to 293.15K. The diffusion parameter of S_8 is taken from Lu et al. [10] with $2.6e^{-10}m^2s^{-1}$. Charge transfer coefficients for each of the electron transfer reactions are chosen to be 0.5. Following the experimental procedure, CV is simulated and recorded for two cycles in a range between 3.8V to 1.0V whereas the evaluated part of the voltammogram is the second cycle. At potentials $<1.8V$, the experimental results show undesired side reactions not included. Diffusion coefficients of all polysulfides as well as reaction constants, formal potentials of the electron transfer reactions and the reaction constants of the chemical reaction are identified to reproduce the experimental data at $100mVs^{-1}$. They are given in Tab. 4. A local availability of S^{2-} is integrated at the electrode/electrolyte interface by choosing an artificially low diffusion coefficient for this species to account for its precipitation at the surface, which is not included in the model. For the here presented reaction kinetic modeling, integrating intricate inhomogeneous precipitation processes would heavily complicate the model and would distract from the focus of identifying the reaction kinetics. To assure quasi steady state of surface and solution, the second scan is used both in experiment and simulation.

6. Results and discussion

In the following, the two proposed kinetic models and their ability and shortcoming to describe the experimentally observed CV is discussed and a parameter sensitivity analysis elucidates the parameter impact. This procedure is first implemented for the EEC_{irr}-mechanism and then repeated for the more complex, physically motivated E3C4-mechanism.

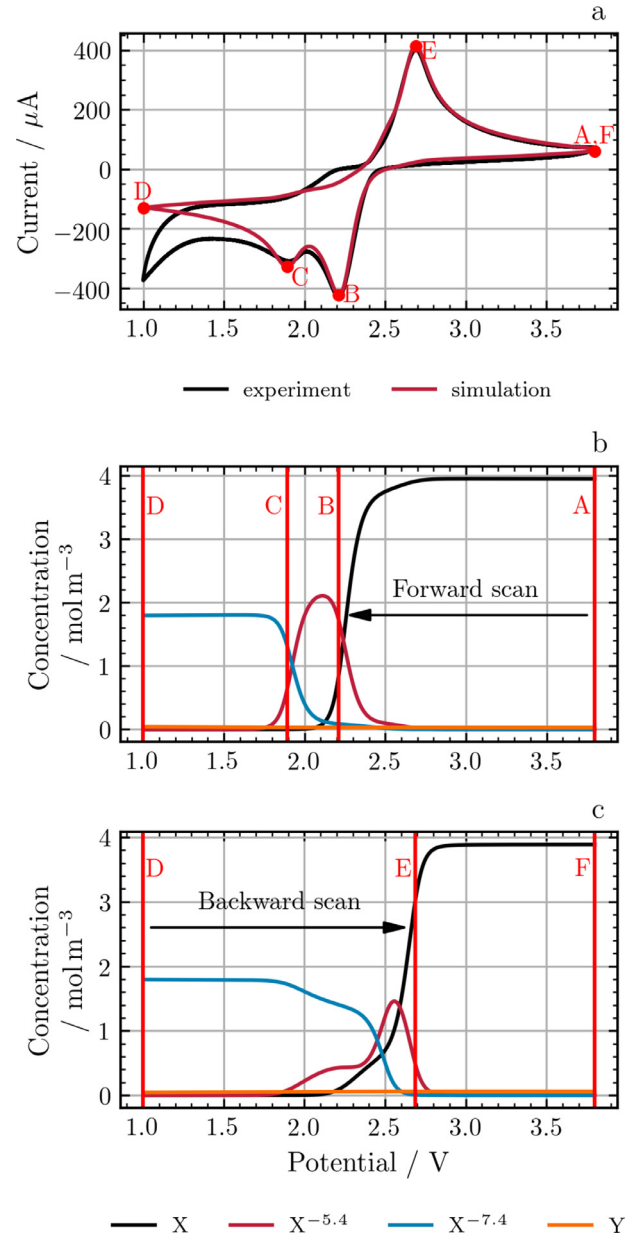


Fig. 3. Cyclic voltammetry results of the EEC_{irr}-mechanism for a scan rate of $\nu = 100mVs^{-1}$. Points A to F indicate significant states of the system (a) Simulated CV compared to experimental results of the 2nd cycle from Schön et al. [11], (b) Concentrations at the surface of the electrode $x_r = 0mm$ during the forward scan and (c) the backward scan.

EEC_{irr}-mechanism

In Fig. 3a the simulated CV of the model with EEC_{irr} kinetic is shown in comparison to the experiment. In addition, characteristic points in the experimental graph are marked from A to F, where B, C and E are points in time which correspond to oxidation and reduction peaks. It can clearly be seen, that the EEC_{irr}-mechanism matches the experiment in good agreement regarding all points except at low potential point D. The behavior at point D deviates significantly which is expected, because it is caused by electrolyte degradation, which is not included in the model. However, two parts of the simulated CV show a different characteristic. First, directly after point C the cathodic current decreases too fast compared with the experiment. The reason for this

behavior is, that in the experiment more electrons per mole of substrate are transferred after the peaks. Second, during the positive scan at a potential of 2.0V, a current approaching zero is expected which can also not be reproduced by the EEC_{irr}-mechanism. Here, the EEC_{irr}-mechanism exhibits a diffusion limited current, while the experimentally observed drop to zero indicates that sulfur (X) is not available at the surface for reduction despite sufficient sulfur concentration in the bulk. This in turn suggests that the mechanism misses a chemical reaction that consumes the reactant in experiments before it reaches the surface. In the following, reactions and concentrations are correlated to elucidate the origin of the CV features and dominant processes.

During the sweep to lower potentials, sulfur (X) is reduced to the intermediate $X^{5.4-}$ and this intermediate gets consecutively reduced to $X^{7.4-}$. The respective change of concentration is shown in Fig. 3b. The concentration of sulfur (X) at the electrode/electrolyte interface drops to zero, while the concentration of $X^{5.4-}$ increases and then it decreases again in favor of the final reduction product $X^{7.4-}$. Reduction of sulfur (X) starts and causes a cathodic current when the potential approaches the formal potential of reaction Ia, which is 2.44V. Similarly, the formal potential of reaction IIa of 2.20V is the potential at which reduction of $X^{5.4-}$ starts and current increases to form the second cathodic peak. At B and C, the concentrations have the highest gradient with respect to potential change. Here, reaction rates are maximal, resulting in the cathodic current peaks. When approaching point D, the concentrations at the surface are nearly constant, indicating a diffusion limitation of X to the electrode/electrolyte interface. At the surface sulfur (X) entirely reacts to $X^{7.4-}$, which diffuses away from the surface with the same magnitude.

When surpassing the formal potential of reaction IIa during the backward scan, the rate of $X^{5.4-}$ conversion to $X^{7.4-}$ decreases, resulting in two effects that are displayed in Fig. 3c. Firstly, the concentration of $X^{7.4-}$ at the electrode/electrolyte interface diminishes because of diffusion. Secondly, the concentration of $X^{5.4-}$ is increasing because the reaction rate Ia is still high at this potential. Reaching point E, reaction Ia stops and the concentration gradients for sulfur (X) and $X^{5.4-}$ with respect to potential pass their maximum resulting in the anodic peak. Finally, when approaching point F, the concentrations at the surface are nearly constant and only few reduced species still exist and diffuse to the surface causing a diffusion limited current.

To elucidate the above seen important role of diffusion in the CV, distinctive concentration profiles of species X, $X^{5.4-}$ and $X^{7.4-}$ vs. distance from the electrode/electrolyte interface are observable from Fig. 4. Sulfur (X) has a concentration minimum between the electrode/electrolyte interface and the bulk, because X is produced from $X^{5.4-}$ by reaction Ia at the end of cycle one and it is sufficiently available in the bulk. After point C, the current is dictated by the delivery of additional X via diffusion from the bulk solution causing a decrease till point D. Due to diffusion the layer at the electrode/electrolyte interface containing the reduced $X^{5.4-}$ and $X^{7.4-}$ continuously grows throughout the scan. Fig. 4 shows, that during dynamic operation reacting species are always in mixture with other species. Therefore, the system behavior always depends on multiple reactions and to the best of our knowledge, analytical solutions are not possible in this case. The courses of concentrations of sulfur (X), $X^{5.4-}$ and $X^{7.4-}$ are almost identical at point A and F indicating the good reversibility of the mechanism at this scan rate.

Chemical reaction IIIa is slow compared to the electron transfer reactions Ia and IIa. This results in a CV that appears reversible. Consequently, the concentration of Y throughout the experiment at all places is negligible, as it can be seen in Fig. 4. The amount of Y produced in the chemical reaction IIIa increases as the scan rate of the experiment decreases, thereby creating a more irreversible

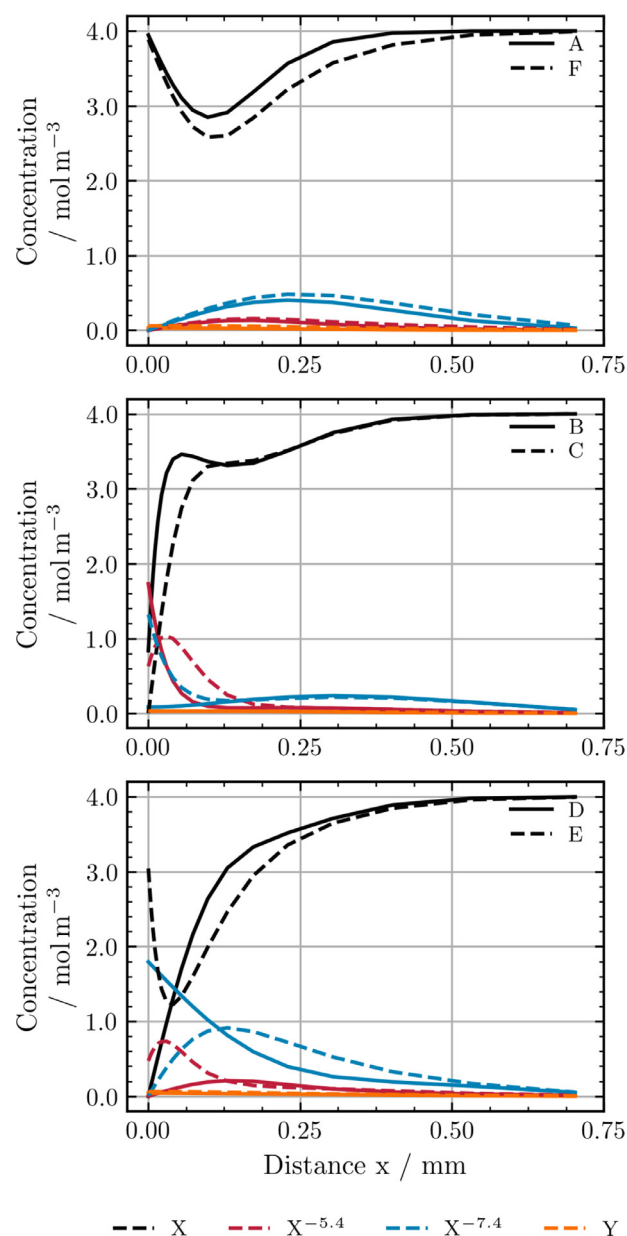


Fig. 4. Concentration profiles of the EEC_{irr}-mechanism during CV simulation with optimized parameters with a scan rate $\nu = 100\text{mVs}^{-1}$ at points A to F. Results are shown for the second cycle.

response of the system. The ratio of the anodic to cathodic peak currents decreases because the reduced species $X^{7.4-}$ is consumed by the subsequent chemical reaction, resulting in fewer species to oxidize on the anodic scan, see Fig. 5.

The sensitivity of each model parameter on the observed current during a CV is displayed in Fig. 6; for direct correlation of the sensitivities with the current at a given potential, the current is also displayed (red line). The sum of all single parameter sensitivities at a given potential sums up to 1, and we thus the single parameter sensitivities (colored bars) stacked on each other. Each parameter sensitivity value represents the relative impact the parameter has on the current at the given potential. Over a wide range of the scan, diffusion of sulfur (X) has the largest impact. When reaching the formal potential of reaction Ia, kinetic parameters dominate and the current gets significantly influenced by the reaction rate constant of reaction Ia, until the first cathodic peak is reached. At the second cathodic peak, the sensitivity of the current

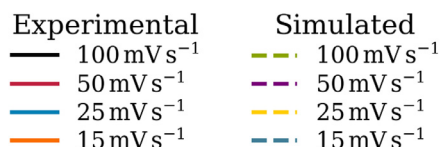
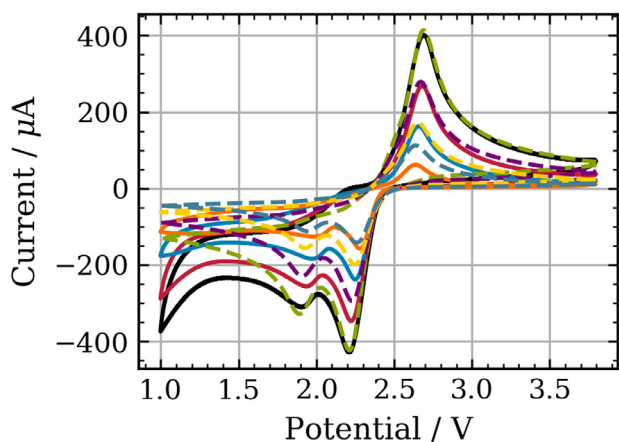


Fig. 5. Comparison of experimental and simulation cyclic voltammetry of the 2nd cycle results vs. potential of the EEC_{irr}-mechanism evaluating scan rate dependency with 100mVs⁻¹, 50mVs⁻¹, 25mVs⁻¹, and 15mVs⁻¹.

to the reaction rate constant of reaction IIa is much lower, because only a small share of the total current is added by reaction IIa. The bigger amount is added by reaction Ia, which explains the remaining strong significance of sulfur (X) diffusion.

In contrast during the backward scan, the anodic peak, displayed in Fig. 6b, is influenced by both reaction rate constants Ia and IIa, because these reactions overlap. The second reaction influences the beginning of the increase, therefore the current is most sensitive to k_{IIa} . When $X^{7.4-}$ concentration rapidly decreases at the surface at ~2.4V, the electron transfer reaction Ia takes over and the sensitivity of k_{Ia} is dominant.

In conclusion, the EEC_{irr}-mechanism is able to achieve qualitative agreement with the experimental data. Pure analytical inves-

tigation of such mechanisms without the here presented macrokinetic modeling is limited as peaks and profiles are overlapping and lead to complex patterns. Therefore, simulation and identification of the parameters, as demonstrated here, is the only way of gaining a complete insight and understanding of the complex interaction of thermodynamic, kinetic and transport properties of the sulfur reaction mechanism through CV. Yet, parts of the experimental CV characteristics are missing. In particular, the EEC_{irr}-mechanism exhibits diffusion limitation, when chemical reactions should be influencing the current. In the following section, a more physically motivated mechanism will be applied to see how the species and reactions proposed in literature interact and, together with diffusion, are able to explain CV behavior of sulfur electrodes.

E3C4-Mechanism

The E3C4-mechanism is primarily characterized by three electron transfer reactions occurring at two different formal potentials: 2.44V for reaction Ib and IIb and 2.3V for reaction IIIb. Compared to the EEC_{irr}-mechanism, the electrons directly transferred by electron transfer reactions differ by $1.4e^- \text{ mol}_S^{-1}$. To compensate this missing charge, chemical reactions Vb, VIb and VIIb are introduced that are able to produce additional S₈. In Fig. 7a the simulation results are shown in comparison to the experiment. A comparison to different scan rates is shown in Fig. A.10. It can clearly be seen, that also this mechanism matches the experiment in good agreement regarding all relevant points. Point F deviates because of experimental electrolyte degradation, as explained earlier. In contrast to the EEC_{irr}-mechanism, the E3C4-mechanism better reproduces the two previously missing features: (i) the slow current decrease directly after point C and (ii) zero current when increasing voltage to 2V.

During the forward scan from 3.8V to 1.0V, S₈ reduces to S₈⁴⁻ via S₈²⁻ when passing the formal potential of reaction Ib and IIb. The intermediate is only present for a short time period, see Fig. 7b. Reactions Ib and IIb overlap, as indicated by the single reaction currents displayed in Fig. 8a. Reaction Ib and IIb are related to the upper potential discharge plateau with a potential >2.3V during galvanostatic discharge. Because of the fast chemical reaction IVb between S₈⁴⁻ and S₄²⁻ (Fig. 7c), these species exhibit a

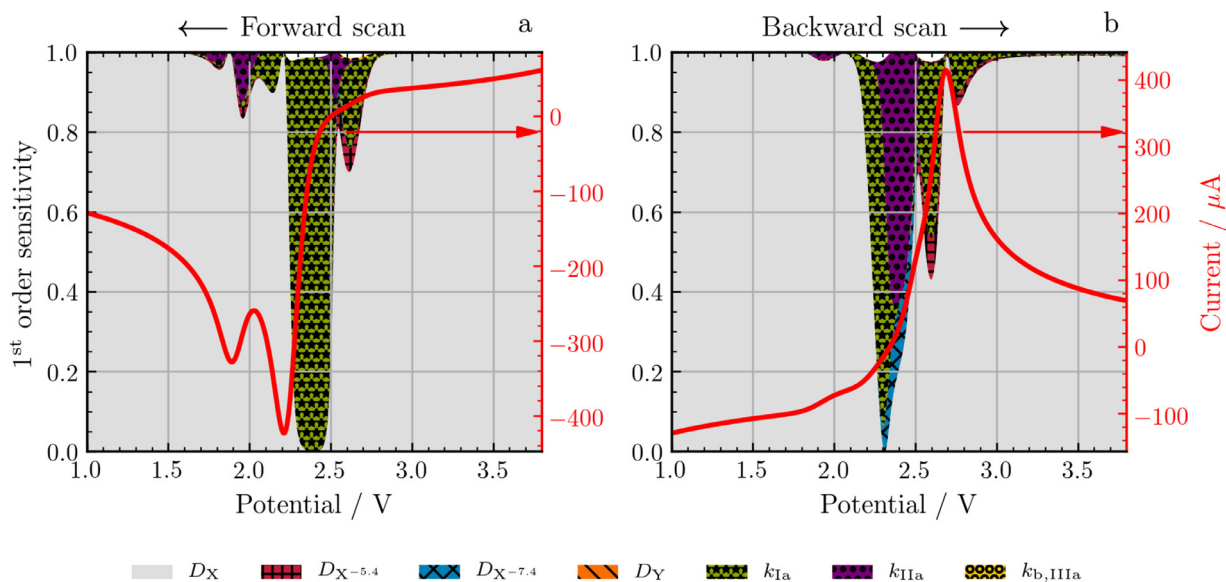


Fig. 6. First order sensitivity results for each parameter influencing the current of the EEC_{irr}-mechanism. The values are stacked as they sum up to 1. The current (red line) is displayed for better correlation to the CV results. 16000 simulations were recorded varying the parameters by $\pm 10\%$. (For interpretation of the references to colour in this figure legend, the reader is referred to the web version of this article.)

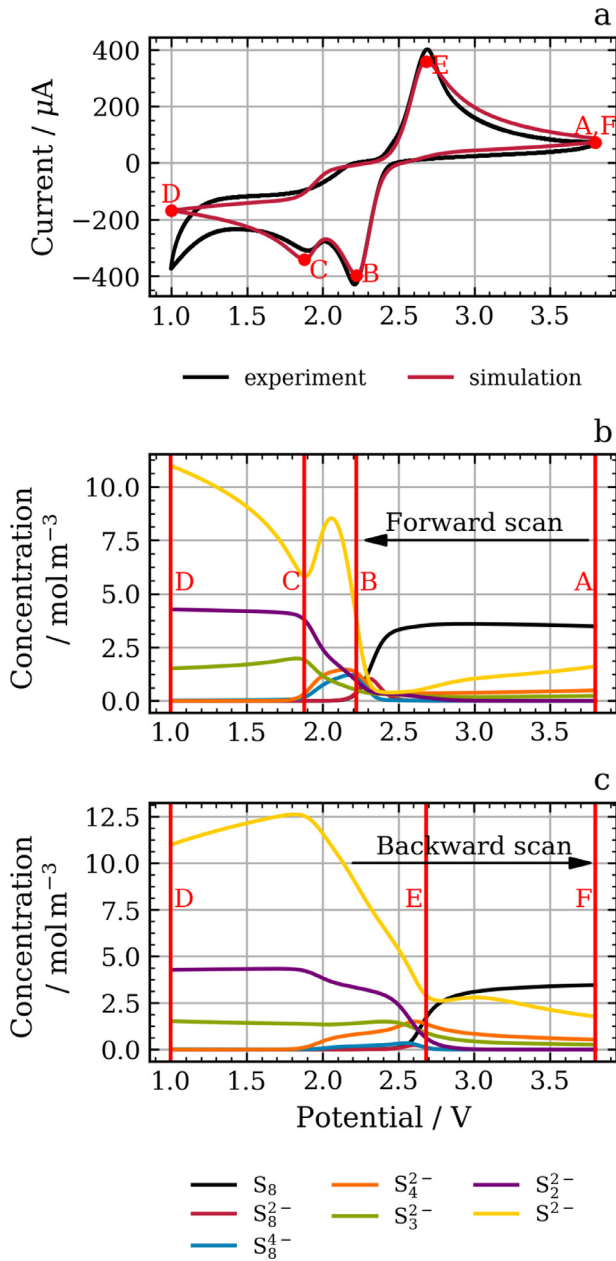


Fig. 7. Cyclic voltammetry results of the E3C4-mechanism for a scan rate of $\nu = 100\text{mVs}^{-1}$. Points A to F indicate significant states of the system and are further analyzed. (a) Simulated cyclic voltammograms of the 2nd cycle compared to experimental results from Schoen et al. 2019 [11] (b) Concentration at the surface of the electrode $x_f = 0\text{mm}$ during the forward scan and (c) the backward scan.

similar course in concentration over potential. In addition, the influence of the circular route through reaction Vb is obvious at a potential of 2.4V. Chemical reaction Vb converts S_4^{2-} back to S_8 and to the smaller molecules S_2^{2-} and S^{2-} . In addition, chemical reactions VIb and VIIb run backward consuming more S_4^{2-} to produce more S_8 . This drives the system to a more reduced state. The here discussed quite complex interplay of the chemical reactions causes the negative and positive reaction rates displayed in Fig. 8b. We thus deduce that the occurring reactions at the higher potential discharge plateau of a LSB can be summarised as follows:

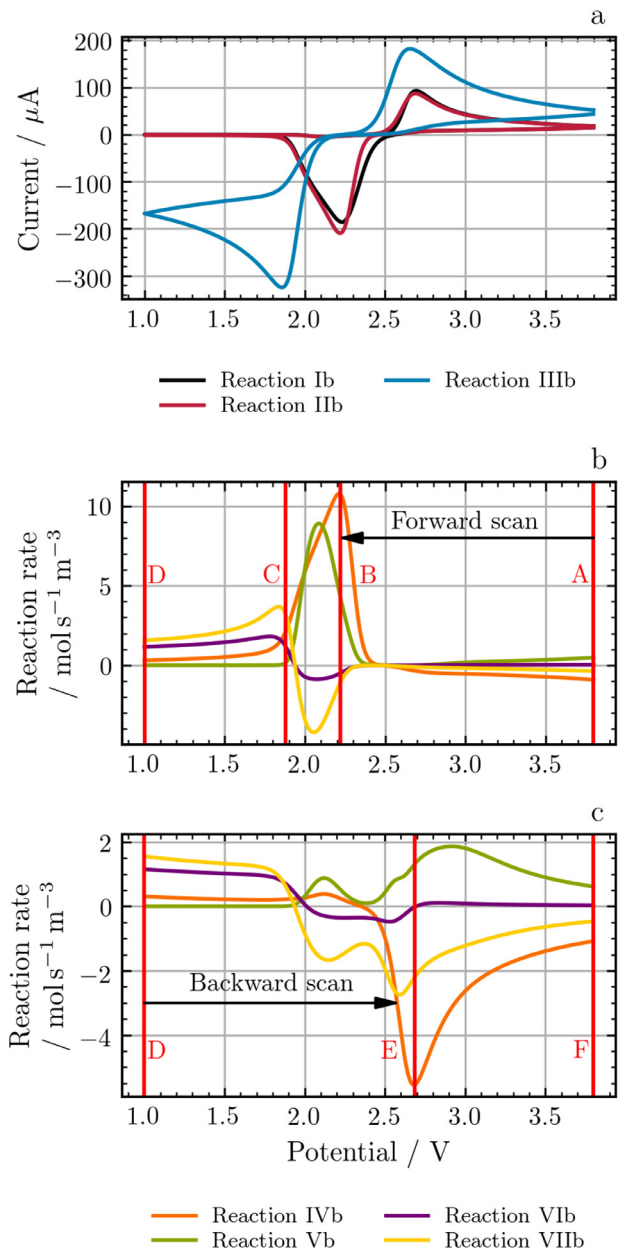
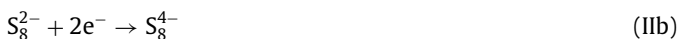


Fig. 8. (a) Reaction currents of the implemented electron transfer reactions of the E3C4-mechanism. (b) Reaction rates of the chemical equilibrium reactions for the forward scan at the electrode surface. (c) Reaction rates of the chemical equilibrium reactions for the backward scan at the electrode surface.



The mechanism also clearly explains the usually observed slow but strong relaxation behaviour in LSBs. Though the mechanism is complex, it agrees well with the large range of polysulfides detected by HPLC analysis starting at 87.1% SoC (Fig. 2).

In the following, the behavior at lower potential is discussed. At $\sim 2.2\text{V}$, the third electron transfer reaction IIIb of reducing S_4^{2-} to

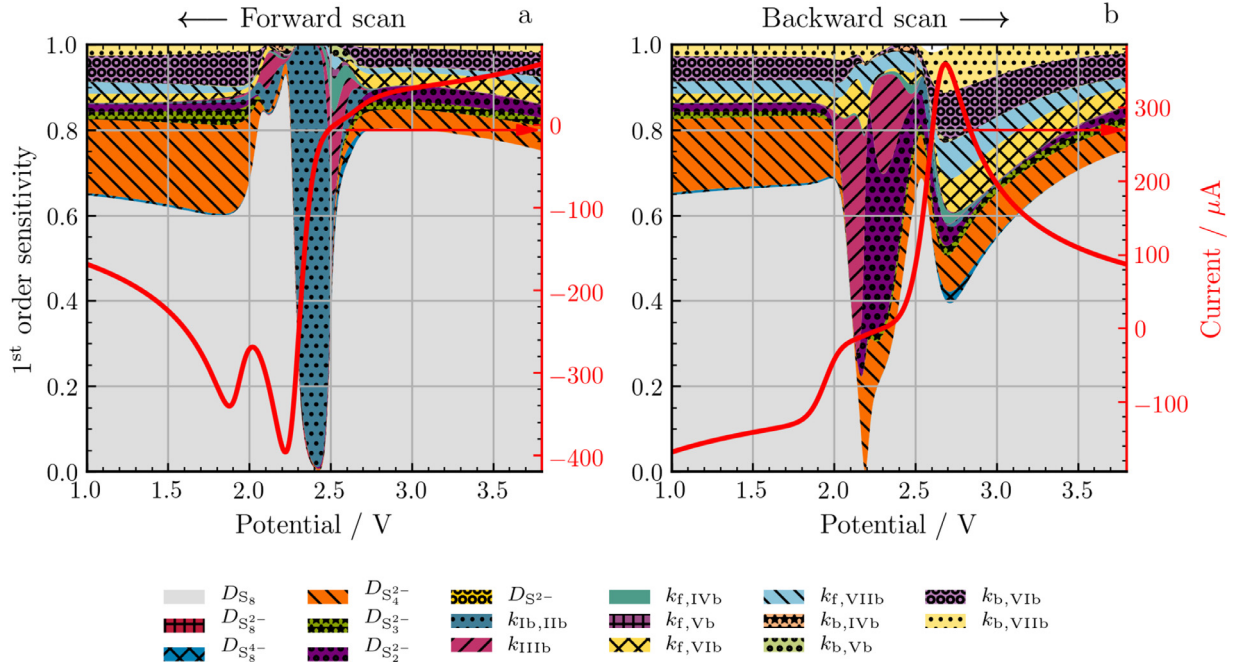
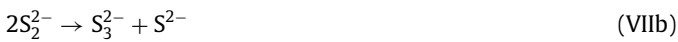


Fig. 9. First order sensitivity results for each parameter influencing the current. The values are stacked as they sum up to 1. The current (red line) is displayed for better correlation to the CV results. 40000 simulations were recorded varying the optimized parameters of Tab. 4 $\pm 10\%$. (For interpretation of the references to colour in this figure legend, the reader is referred to the web version of this article.)

S_2^{2-} kicks in (Fig. 8a). As S_4^{2-} concentration decreases, the competing chemical reaction Vb and so S_8 rapidly decreases. When diffusion diminishes in addition the S_4^{2-} concentration reaction Vb even changes direction and consumes S_8 before it reaches the electrode/electrolyte interface. With both, S_8 and S_8^{4-} concentration being strongly diminished, electron transfer reactions Ib and IIb no longer contribute to the total current when reaching a potential of $\sim 1.8V$. In addition to the reversal of Vb due to missing S_4^{2-} , the reactions VIb and VIIb which convert S_4^{2-} with S_2^{2-} and S^{2-} are reversed as well. In summary, the lower potential discharge plateau starts, when S_8 is no longer present at the electrode/electrolyte interface, and there is a radical change in the mechanism. The only electron transfer reaction that continues is reaction IIIb. A circular route is formed that produces S_4^{2-} for the electrochemical reduction, which is an explanation for the broad CV peaks during the lower potential discharge plateau [11]. This leads to the following reduction mechanism at the electrode/electrolyte interface which will prevail during the lower potential discharge plateau of Li-S cells:



In addition, further away from the electrode/electrolyte interface, S_8 is consumed by reaction Vb, which produces new reactant for reaction IIIb:



This mechanism is much simpler than at high potential but can still explain also the observed relaxation behavior at open circuit voltage [11]. At point D, the reversal point, the system reaches a steady state condition with constant polysulfides compositions, diffusion and constant reaction rates (Fig. 7). In the following we

analyze the positive scan, i.e. the sulfur electrode behavior during charge.

Approaching 2.6V, the electrochemical oxidation sets in, first of reaction IIIb, then IIb and Ib (see Fig. 8a). The reaction rate constant of reaction IIIb is significantly lower than that of reactions Ib and IIb. Thus, the anodic peak potentials of all three electron transfer reactions are close, resulting in one anodic peak. In addition, the chemical reactions Vb, VIb and VIIb support the formation of the oxidizable species S_2^{2-} and therefore ensure more complete oxidation of the system. This can be seen in the large amount of S_2^{2-} over a wide potential range with decreasing S_3^{2-} (Fig. 7c) and the strongly negative rate of VIIb and positive rate of Vb (Fig. 8c). Note that also the S^{2-} decrease is slow due to reproduction by reaction Vb. Following Fig. 8c, the complete set during oxidation at the sulfur electrode is thus:



Similar as for the EEC_{irr}-mechanism, the concentration profiles of S_8 and polysulfides in the electrolyte depend on the potential applied in course of time, see Fig. 4. The concentration of S_8 drops to zero at and close to the electrode/electrolyte interface after the

second reduction peak (points C and D) as S_8 is more rapidly consumed than diffusing from the bulk (compare Fig. A.11).

Thus also in this physicochemical motivated mechanism, diffusion an even more chemical reactions in the bulk play a significant role in explaining the experimentally observed behavior in CV, and will have non negligible and complex impact on sulfur electrode behavior during charge. This will always lead to extremely complex behavior of sulfur electrodes during charge and discharge. Whereas the suggested set of electrochemical and chemical reactions may not be the only possible set explaining the CV, it explains the HPLC and relaxation behavior well, and is thus a robust and suitable choice for analyzing, modeling and understanding typical behavior of sulfur electrodes in DOL/DME electrolyte.

Analyzing the sensitivity of the diffusion coefficients and reaction rate constants of each species and reaction on the current, the result is quite different from the EEC_{irr} -mechanism as it is much more affected by chemical reactions, see Fig. 9. In the kinetic limited area of the reduction reaction from 3.8V to 2.6V, the current is most sensitive to the diffusion of substrate from the bulk to the electrode/electrolyte interface, in this case S_8 . In addition, we observe a notable sensitivity of the diffusion coefficients of the short chain polysulfides, S_4^{2-} , S_3^{2-} and S_2^{2-} , as oxidation of the short polysulfides still takes place. When reaching the first cathodic peak, the electron transfer reactions Ib and IIb show the highest sensitivity impact. This emphasizes, that the current is mainly influenced by these reactions. However as expected, the peak current is almost exclusively sensitive to the S_8 diffusion, as it strongly depends on fresh substrate to be delivered to the electrode/electrolyte interface. The peak current of the second cathodic peak is more affected by diffusion of S_4^{2-} and chemical reactions ($k_{IVb-VIIb}$). These are also important when reaching diffusion limitation. During the reverse scan, in the voltage range of 2.0V to 2.3V, the current's sensitivity on kinetic parameters is very high. This supports the earlier findings, that the introduction of multiple chemical reactions is necessary to reproduce and explain the experimental behaviour of the sulfur electrode. The anodic peak current is strongly affected by chemical reactions, which explains its scan rate dependence that was demonstrated by the irreversible reaction when analyzing the EEC_{irr} -mechanism (Fig. 5). Possible irreversible processes to be included in the future are the precipitation of S_2^{2-} and S^{2-} . Introducing chemical irreversibly of either reaction Vb-VIIb does not lead to the desired result, because the equilibrium of the reaction mechanism gets disturbed.

In summary, the proposed mechanism including electron transfer reactions summarized by Wild et al. [12], and circular routes including the reproduction of S_8 [9–11] shows good agreement of the CV. Compared to the EEC_{irr} -mechanism, introducing a circular route enabled the current increase to zero at 2.0V during the forward scan. This indicates the S_8 consumption before reaching the electrode/electrolyte interface. In addition, the circular route compensates for the missing charge because only $4e^-$ per S_8 are transferred by electron transfer reactions Ib and IIb compared to $5.4e^-$ for the EEC_{irr} -mechanism. In general, the current is greatly influenced by the chemical reactions Vb, VIb and VIIb.

7. Conclusion

In this study the reaction mechanism and kinetics at the sulfur electrode of LSBs is analyzed by physicochemical simulation of CV. Two mechanisms were introduced to evaluate the influence of diffusive transport and interaction of electron transfer and chemical reaction kinetics on the resulting current in a CV experiment. First, the kinetic model based on the EEC_{irr} -mechanism results in the desired reduction and oxidation peaks. It fails reproducing the diffusion limiting current directly after the second cathodic peak and exhibits a cathodic current that is not measured in the exper-

iment when crossing 2.0V during the reverse scan. Nevertheless, this mechanism can be used to replicate general sulfur electrode characteristics, which are two reduction steps and rate dependency due to chemical reactions. However, the application of this mechanism should be restricted to models, where an exact electrolyte composition is irrelevant. Studies of the shuttle mechanism or S^{2-} precipitation should use the physically motivated reaction mechanism to simulate real LSB behaviour.

The second reaction kinetic model uses a more realistic and complex reaction mechanism that incorporates results of several prior research studies from literature. In addition to three electron transfer reactions, chemical reactions of short chain polysulfides have a significant impact on the behavior of the system. Throughout all SoC states, the important role of disproportionation is pointed out while the direction of different reactions and the influence of the reactions on the current varies. Strongly different prevailing reactions on the different discharge plateaus and between reduction and oxidation of the system can be seen, i.e. discharge and charge.

An important feature of the mechanism is the circular route that converts shorter polysulfides to S_8 . It leads to a more reduced state of the products of the higher potential discharge plateau that could not be reproduced by the EEC_{irr} -mechanism. The presence of diverse polysulfides in the electrolyte as seen by the HPLC measurements can only be represented by the complex E3C4-mechanism, which is particularly suitable for more exact investigations of the LSB limitations like the shuttle mechanism or insulation of the electrode by S_8 or S^{2-} precipitation. Our studies emphasise that profound knowledge of the reaction mechanism and its kinetics needed to understand and control the complex electrode behavior and is therefore key to further improve LSB performance. It is proven, that implementation of solely electron transfer reactions in LSB models is not sufficient to reproduce the real behavior of a LSB. Future model-supported studies will exceedingly benefit when dealing with degradation, optimization of electrolyte composition or prevention of passivating surfaces. In addition, improvements in cell control can be expected, with overall higher voltages and better sulfur utilization, which directly increases the cell capacity. However, more work has to be done to gain comprehensive results of different LSB systems, where various electrolytes and electrode materials are used. And thus other reactions may prevail and cause different effects.

Declaration of Competing Interest

The authors declare that they have no known competing financial interests or personal relationships that could have appeared to influence the work reported in this paper.

Supplementary material

Supplementary material associated with this article can be found, in the online version, at [10.1016/j.electacta.2020.137523](https://doi.org/10.1016/j.electacta.2020.137523).

Credit authorship contribution statement

Patrick Schön: Conceptualization, Methodology, Software, Validation, Formal analysis, Investigation, Writing - original draft, Visualization. **Ulrike Krewer:** Conceptualization, Methodology, Writing - review & editing, Supervision, Project administration, Funding acquisition.

References

- [1] A. Fotouhi, D.J. Auger, L. O'Neill, T. Cleaver, S. Walus, Lithium-sulfur battery technology readiness and applications-a review, *Energies* 10 (12) (2017) 1937.

- [2] J. Chen, F. Cheng, Combination of lightweight elements and nanostructured materials for batteries, *Acc. Chem. Res.* 42 (6) (2009) 713–723.
- [3] C. Li, H. Zhang, L. Otaegui, G. Singh, M. Armand, L.M. Rodriguez-Martinez, Estimation of energy density of li-s batteries with liquid and solid electrolytes, *J. Power Sources* 326 (2016) 1–5.
- [4] M. Hagen, D. Hanselmann, K. Ahlbrecht, R. Maça, D. Gerber, J. Tübke, Lithium-sulfur cells: the gap between the state-of-the-art and the requirements for high energy battery cells, *Adv. Energy Mater.* 5 (16) (2015) 1401986.
- [5] Y.V. Mikhaylik, J.R. Akridge, Polysulfide shuttle study in the li/s battery system, *J. Electrochem. Soc.* 151 (11) (2004) A1969–A1976.
- [6] Y. Diao, K. Xie, S. Xiong, X. Hong, Shuttle phenomenon—the irreversible oxidation mechanism of sulfur active material in li-s battery, *J. Power Sources* 235 (2013) 181–186.
- [7] J. Yan, X. Liu, B. Li, Capacity fade analysis of sulfur cathodes in lithium-sulfur batteries, *Adv. Sci.* 3 (12) (2016) 1600101.
- [8] M. Barghamadi, A.S. Best, A.I. Bhatt, A.F. Hollenkamp, M. Musameh, R.J. Rees, T. Rütger, Lithium-sulfur batteries—the solution is in the electrolyte, but is the electrolyte a solution? *Energy & Environmental Science* 7 (12) (2014) 3902–3920.
- [9] Y. Jung, S. Kim, B.-S. Kim, D.-H. Han, S.-M. Park, J. Kwak, Effect of organic solvents and electrode materials on electrochemical reduction of sulfur, *Int. J. Electrochem. Sci.* 3 (5) (2008) 566–577.
- [10] Y.-C. Lu, Q. He, H.A. Gasteiger, Probing the lithium-sulfur redox reactions: arotating-ring disk electrode study, *The Journal of Physical Chemistry C* 118 (11)(2014) 5733–5741.
- [11] P. Schön, F. Hintz, U. Krewer, Electrochemical analysis of the reaction mechanism of sulfur reduction as a function of state of charge, *Electrochim. Acta* 295 (2019) 926–933.
- [12] M. Wild, L. O'Neill, T. Zhang, R. Purkayastha, G. Minton, M. Marinescu, G.J. Offer, Lithium sulfur batteries, a mechanistic review, *Energy and Environmental Science* 8 (12) (2015) 3477–3494.
- [13] T. Cleaver, P. Kovacic, M. Marinescu, T. Zhang, G. Offer, Perspective—commercializing lithium sulfur batteries: are we doing the right research? *J. Electrochem. Soc.* 165 (1) (2018) A6029–A6033.
- [14] K. Propp, M. Marinescu, D.J. Auger, L. O'Neill, A. Fotouhi, K. Somasundaram, G.J. Offer, G. Minton, S. Longo, M. Wild, V. Knap, Multi-temperature state-dependent equivalent circuit discharge model for lithium-sulfur batteries, *J. Power Sources* 328 (2016) 289–299.
- [15] T. Zhang, M. Marinescu, S. Walus, G.J. Offer, Modelling transport-limited discharge capacity of lithium-sulfur cells, *Electrochim. Acta* 219 (2016) 502–508.
- [16] V. Knap, D.-I. Stroe, M. Swierczynski, R. Purkayastha, K. Propp, R. Teodorescu, E. Schaltz, A self-discharge model of lithium-sulfur batteries based on direct shuttle current measurement, *J. Power Sources* 336 (2016) 325–331.
- [17] M. Marinescu, T. Zhang, G.J. Offer, A zero dimensional model of lithium-sulfur batteries during charge and discharge, *PCCP* 18 (1) (2016) 584–593.
- [18] K. Kumaresan, Y. Mikhaylik, R.E. White, A mathematical model for a lithium-sulfur cell, *J. Electrochem. Soc.* 155 (8) (2008) A576–A582.
- [19] D. Moy, A. Manivannan, S.R. Narayanan, Direct measurement of polysulfide shuttle current: a window into understanding the performance of lithium-sulfur cells, *J. Electrochem. Soc.* 162 (1) (2015).
- [20] A.F. Hofmann, D.N. Fronczek, W.G. Bessler, Mechanistic modeling of polysulfide shuttle and capacity loss in lithium-sulfur batteries, *J. Power Sources* 259 (2014) 300–310.
- [21] U. Krewer, M. Christov, T. Vidakovic, K. Sundmacher, Impedance spectroscopic analysis of the electrochemical methanol oxidation kinetics, *J. Electroanal. Chem.* 589 (1) (2006) 148–159.
- [22] Q. Mao, U. Krewer, Total harmonic distortion analysis of oxygen reduction reaction in proton exchange membrane fuel cells, *Electrochim. Acta* 103 (2013) 188–198.
- [23] F. Kubannek, C. Moß, K. Huber, J. Overmann, U. Schröder, U. Krewer, Concentration pulse method for the investigation of transformation pathways in a glycerol-fed bioelectrochemical system, *Front. Energy Res.* 6 (2018) 125.
- [24] I.M. Sobol, Global sensitivity indices for nonlinear mathematical models and their monte carlo estimates, *Math. Comput. Simul.* 55 (1–3) (2001) 271–280.
- [25] A. Saltelli, Making best use of model evaluations to compute sensitivity indices, *Comput. Phys. Commun.* 145 (2) (2002) 280–297.
- [26] A. Saltelli, P. Annoni, I. Azzini, F. Campolongo, M. Ratto, S. Tarantola, Variance based sensitivity analysis of model output. design and estimator for the total sensitivity index, *Comput. Phys. Commun.* 181 (2) (2010) 259–270.
- [27] J. Crank, *The mathematics of diffusion*, Oxford university press, 1979.
- [28] A.W. Bott, S.W. Feldberg, M. Rudolph, Fitting experimental cyclic voltammetry data with theoretical simulations using digisim [r] 2.1, *Curr. Sep.* 15 (1996) 67–71.
- [29] L.K. Bieniasz, Elsim—a problem-solving environment for electrochemical kinetic simulations. version 3.0—solution of governing equations associated with interfacial species, independent of spatial coordinates or in one-dimensional space geometry, *Computers & chemistry* 21 (1) (1997) 1–12.
- [30] M. Rudolph, Attaining exponential convergence for the flux error with second and fourth order accurate finite difference equations. i. presentation of the basic concept and application to a pure diffusion system, *J. Comput. Chem.* 26 (6) (2005) 619–632.
- [31] C. Nervi, *Esp electrochemical simulation package*, 1994.
- [32] J.H. Brown, Development and use of a cyclic voltammetry simulator to introduce undergraduate students to electrochemical simulations, *J. Chem. Educ.* 92 (9) (2015) 1490–1496.
- [33] S. Wang, J. Wang, Y. Gao, Development and use of an open-source, user-friendly package to simulate voltammetry experiments, *J. Chem. Educ.* 94 (10) (2017) 1567–1570, doi:10.1021/acs.jchemed.6b00986.
- [34] N. Eliaz, E. Gileadi, *Physical electrochemistry: Fundamentals, techniques, and applications*, Wiley-Vch, 2018.
- [35] R.G. Compton, C.E. Banks, *Understanding cyclic voltammetry*, World Scientific, 2018.
- [36] S.D. Cohen, A.C. Hindmarsh, P.F. Dubois, Cvode, a stiff/nonstiff ode solver in c, *Computers in physics* 10 (2) (1996) 138–143.
- [37] A.C. Hindmarsh, P.N. Brown, K.E. Grant, S.L. Lee, R. Serban, D.E. Shumaker, C.S. Woodward, Sundials: suite of nonlinear and differential/algebraic equation solvers, *ACM Transactions on Mathematical Software (TOMS)* 31 (3) (2005) 363–396.
- [38] C.F. Curtiss, J.O. Hirschfelder, Integration of stiff equations, *Proc. Natl. Acad. Sci. U.S.A.* 38 (3) (1952) 235.
- [39] Y. Saad, M.H. Schultz, Gmres: a generalized minimal residual algorithm for solving nonsymmetric linear systems, *SIAM Journal on scientific and statistical computing* 7 (3) (1986) 856–869.
- [40] S. Andersson, C. Führer, J. Åkesson, Assimulo: a unified framework for ode solvers, *Math. Comput. Simul.* 116 (2015) 26–43.
- [41] J.D. Herman, W. Usher, Salib: an open-source python library for sensitivity analysis., *J. Open Source Software* 2 (9) (2017) 97.
- [42] D. Zheng, X. Zhang, C. Li, M.E. McKinnon, R.G. Sadok, D. Qu, X. Yu, H.-S. Lee, X.-Q. Yang, D. Qu, Quantitative chromatographic determination of dissolved elemental sulfur in the non-aqueous electrolyte for lithium-sulfur batteries, *J. Electrochem. Soc.* 162 (1) (2015) A203–A206.
- [43] C. Barchasz, F. Molton, C. Duboc, J.-C. Leprêtre, S. Patoux, F. Alloin, Lithium/sulfur cell discharge mechanism: an original approach for intermediate species identification, *Anal. Chem.* 84 (9) (2012) 3973–3980.
- [44] A. Kawase, S. Shirai, Y. Yamoto, R. Arakawa, T. Takata, Electrochemical reactions of lithium-sulfur batteries: an analytical study using the organic conversion technique, *PCCP* 16 (20) (2014) 9344–9350.
- [45] D. Zheng, D. Liu, J.B. Harris, T. Ding, J. Si, S. Andrew, D. Qu, X.-Q. Yang, D. Qu, Investigation of the li-s battery mechanism by real-time monitoring of the changes of sulfur and polysulfide species during the discharge and charge, *ACS applied materials & interfaces* 9 (5) (2016) 4326–4332.
- [46] D. Zheng, D. Qu, X.-Q. Yang, X. Yu, H.-S. Lee, D. Qu, Quantitative and qualitative determination of polysulfide species in the electrolyte of a lithium-sulfur battery using hplc esi/ms with one-step derivatization, *Adv. Energy Mater.* 5 (16) (2015) 1401888.
- [47] D. Zheng, X. Zhang, J. Wang, D. Qu, X. Yang, D. Qu, Reduction mechanism of sulfur in lithium-sulfur battery: from elemental sulfur to polysulfide, *J. Power Sources* 301 (2016) 312–316.
- [48] D. Zheng, D. Qu, Chromatographic separation of polysulfide species in non-aqueous electrolytes—revisited, *J. Electrochem. Soc.* 161 (6) (2014) A1164–A1166.
- [49] A. Kamyshny, A. Goifman, J. Gun, D. Rizkov, O. Lev, Equilibrium distribution of polysulfide ions in aqueous solutions at 25 °c: A new approach for the study of polysulfides' equilibria, *Environmental Science & Technology* 38 (24) (2004) 6633–6644.
- [50] M. Cuisinier, P.-E. Cabelguen, S. Evers, G. He, M. Kolbeck, A. Garsuch, T. Bolin, M. Balasubramanian, L.F. Nazar, Sulfur speciation in li-s batteries determined by operando x-ray absorption spectroscopy, *J. Phys. Chem. Lett.* 4 (19) (2013) 3227–3232.
- [51] Y. Gorlin, M.U.M. Patel, A. Freiberg, Q. He, M. Piana, M. Tromp, H.A. Gasteiger, Understanding the charging mechanism of lithium-sulfur batteries using spatially resolved operando x-ray absorption spectroscopy, *J. Electrochem. Soc.* 163 (6) (2016) A930–A939, doi:10.1149/2.0631606jes.